 doi:10.20944/preprints202210.0308.v1

Type of the Paper (Article)

CHRDL1 regulates stemness in glioma stem-like cells

Inka Berglar[1], Stephanie Hehlgans[2], Franz Rödel[2,3,4], Donat Kögel[1,3] and Benedikt Linder[1]

[1] Experimental Neurosurgery, Department of Neurosurgery, Neuroscience Center, Goethe University Hospital, 60590 Frankfurt am Main, Germany; inkaberglar@yahoo.de (IB), koegel@em.uni-frankfurt.de (DK), linder@med.uni-frankfurt.de (BL)

[2] : Department of Radiotherapy and Oncology, Goethe University Hospital, 60590 Frankfurt am Main, Germany; Stephanie.Hehlgans@kgu.de (SH), Franz.Roedel@kgu.de (FR)

[3] : German Cancer Consortium DKTK Partner site Frankfurt/Main, 60590 Frankfurt am Main, Germany and German Cancer Research Center DKFZ, 69120 Heidelberg, Germany

[4] : Frankfurt Cancer Institute (FCI), Theodor-Stern-Kai 7, University of Frankfurt, 60590 Frankfurt, Germany

* Correspondence: linder@med.uni-frankfurt

Abstract: Glioblastoma (GBM) still presents as one of the most aggressive tumors in the brain, which despite enormous research efforts remains incurable until today. As many theories evolve around the persistent recurrence of this malignancy the assumption of a small population of cells with a stem-like phenotype remains as a key driver of its infiltrative nature. In this article we research Chordin-like 1 (CHRDL1), a secreted protein, as a potential key regulator of the glioma stem-like cell (GSC) phenotype. It has been shown that CHRDL1 antagonizes the function of Bone Morphogenic Protein 4 (BMP4), which induces GSC differentiation and hence reduces tumorigenicity. We therefore employed two previously described GSCs spheroid cultures and depleted them of CHRDL1 using stable transduction of a CHRDL1-targeting shRNA. We show with in vitro cell based assays (MTT, limiting dilution and sphere formation assays), western blots, irradiation procedures and quantitative real-time PCR that depletion of the secreted BMP4 antagonist CHRDL1 prominently decreases functional and molecular stemness traits resulting in enhanced radiation sensitivity. As a result, we postulate CHRDL1 as an enforcer of stemness in GSCs and find additional evidence that high CHRDL1-expression might also serve as a marker protein to determine BMP4-susceptibility.

Keywords: Glioma, Glioblastoma, Glioma stem-like cells, CHRDL1, BMP4

1. Introduction

Glioblastoma (GBM) is highly aggressive and the most common brain tumor in adults. According to WHO criteria it is classified as a grade 4 astrocytoma [1,2] and despite an intensive treatment regimen consisting of maximally possible surgery followed by radiochemotherapy using the alkylating agent Temozolomide the median survival barely exceeds one year [3-6]. One key characteristic of GBM is its highly infiltrative growth which makes relapses virtually unavoidable [7]. It is hypothesized that recurrences are further supported by tumor cells that can transiently obtain a stem-like phenotype. These glioma stem-like cells (GSCs) [8-10] or tumor-initiating cells are thought to be able to replenish the entire tumor and are considered particularly resistant against conventional therapy including radiotherapy and chemotherapy [11-13]. It has been further shown that these cells reside in specific niches, namely hypoxic or perivascular areas and express proteins associated with stemness, whereas they lack protein expression associated with differentiated neuronal cells [12,14-18]

Recently, we demonstrated that Arsenic trioxide (ATO) efficiently induces differentiation of GSCs and inhibits proliferation, while inducing cell death particularly in combination with the natural anticancer component (-)-Gossypol (Gos, also known as AT-101) [19]. A proteomic analysis further revealed that multiple processes associated with DNA repair, but also associated with stemness were effectively depleted. Among these proteins we identified Chordin-like 1 (CHRDL1) as a potential key regulator of the GSC phenotype.

Preprints (www.preprints.org) | NOT PEER-REVIEWED | Posted: 20 October 2022 doi:10.20944/preprints202210.0308.v1

CHRDL1 is a secreted protein that antagonizes the function of Bone Morphogenic Protein 4 (BMP4) by binding to its receptors [20]. BMP4 in turn has been shown to induce GSC differentiation and reduce tumorigenicity upon transplantation of BMP4-treated GBM cells into nude mice[21]. Additionally, it has been proposed that BMP4-treatment of GSCs induces asymmetric divisions favoring stem-like daughter cells [22], while Sachdeva et al. propose that BMP signaling mediated by BMP4-treatment induces quiescence [23]. Notably, BMP proteins are antagonized by secreted proteins of the Chordin family [24] including CHRDL1 [25]. In particular, Cyr-Depauw et al. showed that CHRDL1 inhibits migration and invasion of breast cancer cells via CHRDL1-mediated BMP4 inhibition [25]. Interestingly, Gao et al. employed rat neural stem cells and demonstrated that CHRDL1 induces neuronal differentiation [26]. We therefore hypothesized that CHRDL1 acts as a GSC-derived inhibitor of BMP4 and thereby maintains GSC stemness. In this study, we show that depletion of the secreted BMP4 antagonist prominently decreases functional and molecular stemness traits resulting in enhanced radiation sensitivity.

2. Materials and Methods

2.1 Cells and Cell Culture

The experiments were conducted with the following glioma stem-like (GSC) lines: NCH644 [27] and GS-5 [28]. All cell lines were maintained in neurobasal medium (Gibco, Darmstadt, Germany). The medium was supplemented with 1 × B27, 100 U/mL Penicillin 100 µg/mL Streptomycin (P/S, Gibco), 1 × GlutaMAX (Gibco), 20 ng/mL epidermal growth factor (EGF, Peprotech, Hamburg, Germany) and 20 ng/mL fibroblast growth factor (FGF, Peprotech) and 2 µg/µl or 0.5 µg/µl Puromycin (Santa Cruz Biotechnology Inc., Heidelberg, Germany), respectively. The GSCs were dissociated using accutase (Sigma-Aldrich, Taufkirchen, Germany) to create a single cell suspension prior to seeding. All cells are tested monthly for mycoplasma using the PCR Mycoplasma Test Kit II (AppliChem, Darmstadt, Germany) according to the manufacturer's instructions. Christel Herold-Mende (University Hospital Heidelberg, Germany) provided NCH644 and GS-5 were gifted by Katrin Lamszus (UKE, Hamburg, Germany). Both lines were generated from surgical specimens using mechanical and enzymatic dissociation and cultivation as free-floating spheroids as described [27,28]. HEK293T (ATCC #CRL-3216) was cultured in Dulbecco's modified Eagle's medium (DMEM GlutaMAX) supplied with heat-inactivated 10% FBS and P/S (all from Gibco).

2.2 Lentiviral Transduction of GSCs

Lentiviral transduction of shRNA targeting CHRDL1 (shCHRDL1) or non-mammalian targeting Control-shRNA (shCtrl) was performed as described previously [29,30] after transfection of the shRNA-containing vector (pLKO.1-puro, Sigma-Aldrich), gag/pol-plasmid (psPAX2, addgene #12260) and VSV-G envelope plasmid (pMD2.G, addgene #12259) into HEK293T cells. Viral supernatants were collected after 16h and additionally after 24h pooled and mixed with fresh medium (ratio: 1:1) supplied with 8 µg/mL protamine sulfate (Sigma-Aldrich) immediately prior to transduction. To select for positively transduced cells 2 µg/mL and 0.5 µg/mL puromycin were added and maintained in the culture 48h post-transduction for NCH644 and GS-5, respectively. pLKO.1-puro plasmids containing the shCHRDL1 or shCtrl (SHC002)-sequences were purchased from Sigma-Aldrich. To deplete CHRDL1 one the following sequences were used:

3'-CCGGGAGAACTGTCATGGGAACATTCTCGAGAATGTTCCCATGACAG-TTCTCTTTTTTG-5'(TRCN0000149739) and

3'- CCGGACGCCATGCACAGCATAATTTCTCGAGAAATTATGCTGTG-CATGGCGTTTTTTG-5'(TRCN0000371790) for NCH644 and GS-5, respectively.

Preprints (www.preprints.org) | NOT PEER-REVIEWED | Posted: 20 October 2022 doi:10.20944/preprints202210.0308.v1

2.3 Cell-Based Assays

2.3.1 MTT (3-(4,5-Dimethylthiazol-2-yl)-2,5-diphenyltetrazolium bromide) assay

MTT assay was performed as described previously [31] and measured on a Tecan Spark (Tecan, Männedorf , Switzerland) plate reader at 560 nm. MTT (Sigma-Aldrich) was solved in sterile PBS at 5 mg/mL. For NCH644, 8,000 cells per well were seeded for 5 time points in a 96-well plate.

2.3.2 Limiting Dilution Assay

The limiting dilution assay (LDA) was performed as described previously [19,32]. To summarize, 96-well plates were used to seed the cells in 200 µL culture medium per well. By performing a row-wise descending dilution, cell concentrations of 8, 16, 32, 64, 128, 256, 512 and 1,024 cells/well for NCH644 and 16, 32, 64, 128, 256, 512, 1,024 and 2,048 cells/well for GS-5 were reached. Stem-cell frequencies were assessed 7 days (NCH644) and 7 and 14 days (GS-5) after seeding using extreme limiting dilution analysis (ELDA) software using the standard settings (http://bioinf.wehi.edu.au/software/elda; [33]; last access on 2022-09-05).

2.3.3 Sphere Formation Assays

To measure the sphere forming ability an assay (SFA) based on Gilbert et al. [34] was performed. Briefly, 500 and 1,000 dissociated NCH644 and GS-5, respectively, were seeded in 96 well plates and measured after 7 days. Images were acquired using a Tecan Spark plate reader and analyzed using a self-developed macro via FIJI (v1.52p) [35] enhancing contrasts and identifying sphere area and properties as described previously [29].

2.4 SDS-PAGE and Western Blot

Western Blotting was carried out as described previously [36]. After blocking with 5% bovine serum albumin (Carl Roth GmbH, Karlsruhe, Germany) (BSA)/Tris-buffered saline (TBS)-Tween 20 (TBS-T) or 5% dry milk (Carl Roth GmbH)/TBS-T, the primary antibodies were incubated overnight in 5% BSA/TBS-T at 4 °C, while secondary goat anti-mouse, goat anti-rabbit or donkey anti-goat antibodies (dilution 1:10,000, LI-COR Biosciences, Bad Homburg, Germany) were incubated at room temperature (RT) for 1h. Detection and quantification was achieved using a LI-COR Odyssey reader (LI-COR Biosciences, Bad Homburg, Germany).

The following primary antibodies and dilutions were used: CHRDL1 (#AF1808, R&D Systems, Wiesbaden-Nordenstadt, Germany) 1:2,000; GAPDH (#CB1001, Calbiochem, Darmstadt, Germany) 1:20,000; SMAD1 [(#6944, Cell Signaling)] 1:1,000; SMAD5 [(#12534, Cell Signaling)] 1:1,000; pSMAD1/5 [(#9516, Cell Signaling)] 1:1,000.

The following secondary antibodies were used at a dilution of 1:10,000 (all from LI-COR Biosciences): IRDye 800CW goat-anti rabbit 1:10,000 (926-32211), IRDye 680RD goat-anti mouse 1:10,000 (926-68070), IRDye® 800CW donkey anti-goat 1:10,000 (926-32214).

2.5 Irradiation Procedures

In total, 500 cells/well were seeded into 96-well plates and irradiated the next day. Irradiation (IR) with single doses of 2, 4 or 6 Gy was performed using a linear accelerator with 6 MV photon energy, 100 cm focus to isocentre distance and a dose rate of 6 Gy/min (Synergy ,Elekta, Crawley, UK) at the Department of Radiation and Oncology (University Hospital Frankfurt, Frankfurt, Germany).

2.6 Immunofluorescence Microscopy / Foci Assay

For DNA damage analyses, NCH644 12,000 cells/well were seeded on Laminin-coated 8-well chamber slides (Falcon, Corning, Amsterdam, NY, USA). Laminin-coating (10 µg/mL, Sigma-Aldrich, L2020) was performed at 4 °C overnight. One day after seeding, the cells were irradiated as indicated and after an additional 24 hours fixed with 4%

Preprints (www.preprints.org) | NOT PEER-REVIEWED | Posted: 20 October 2022 doi:10.20944/preprints202210.0308.v1

paraformaldehyde for 20 min at RT. The slides were washed with TBS-Tween (0.1%; TBS-T), blocked with 4% BSA in TBS with 0.3% Triton X-100 for 1 h at RT and primary antibody incubation occurred at 4 °C overnight. Hereafter, the slides were washed at least three times with TBS-T and secondary antibody was diluted 1:500 in TBS-T and incubated for 1 h at RT. After an additional wash step with TBS-T the slides were mounted with DAPI containing Immunoselect antifading mounting medium (Dianova, Hamburg, Germany) or Fluoroshield with DAPI (Thermo Fisher, Frankfurt, Germany). Images were acquired with an Eclipse TS100 inverted fluorescence microscope (Nikon, Düsseldorf, Germany) operated by NIS Elements AR software (version 3.22, Nikon).

The following primary and secondary antibodies were used: 53BP1 (NP-100-304, Bio-Techne GmbH, Wiesbaden, Germany), 1:1000; Alexa Fluor® 488 F(ab')2 fragment goat anti-rabbit IgG (H+L) (Thermo Fisher); 1:500.

2.7 Taqman-based qRT-PCR

In total, 300,000 cells/well (NCH644) and 600,000 cells/well (GS-5) were seeded into 6-well plates and cells were collected the following day. Experiments were performed using 3 biological replicates for each treatment condition, while the experiment was repeated three times. RNA was isolated using the ExtractMe Total RNA Kit (Blirt S.A., Gdanks, Poland), and 1–2 µg RNA was used for cDNA synthesis. SuperScript III System (Life technologies, Darmstadt, Germany) allowed the synthesis of cDNA, with 100 U per sample to be sufficient. The quantitative Real-Time PCR (qRT-PCR) was performed using Taqman-probes (Applied Biosystems, Darmstadt, Germany), Fast-Start Universal Probe Master Mix (Roche) on a StepOne Plus System (Applied Biosystems) in a 20 µL reaction volume.

Ct values were normalized to TATA box-binding protein (TBP). Fold-change in gene expression was determined by $2^{-\Delta\Delta Ct}$ method.

The following Taqman-probes were used: CHRDL1 (Hs01035484_m1), OLIG2 (Hs00300164_s1), SOX2 (Hs01053049_s1), SOX9 (Hs00165814_m1), ZEB1 (Hs01566408_m1), ZEB2 (Hs00207691_m1), CD44 (Hs01075864_m1), NES (Hs04187831_g1), GFAP (Hs00909233_m1), NEFL (Hs00196245_m1), MAP2 (Hs00258900_m1), RBFOX3 (Hs01370654_m1) and TBP (Hs00427620_m1).

2.8 Interrogation of the human protein atlas

The human protein atlas (proteinatlas.org; last accessed on: 10/10/2022) [37] was accessed using a web browser and the expression of CHRDL1 was analysed among multiple cancer entities. For generation of Kaplan-Meier plots the "Best expression cut-off" was chosen and the reported p-value (log-rank-test) is presented in each sub-figure.

2.9 Statistics

Statistical analyses involved one-way and two-way ANOVA using GraphPad Prism 7 (GraphPad Software, La Jolla, CA, USA), with the respective post hoc test, as indicated. For LDA, the statistical evaluation was taken from ELDA software, which calculated statistical significance based on a chi-square test [33]. Significances were marked as follows: $p < 0.05$: *, $p < 0.01$: **, $p < 0.001$: ***, $p < 0.0001$: ****, ns: not significant.

3. Results

3.1. CHRDL1 depletion reduces stemness of GSCs

To analyze the role of CHRDL1 in maintaining the GSC phenotype, we first established stable CHRDL1-knockdown (KD) cell lines (shCHRDL1) by lentiviral transduction with two different shRNAs directed against CRHDL1. We could show for both, NCH644 [27] (Fig. 1A) and GS-5 [28] (Fig. 1A), that a successful KD could be achieved. Based on our hypothesis that CHRDL1 maintains stemness, we next investigated the sphere forming potential of both GSCs via LDAs. For NCH644 shCtrl (Fig. 1B) we observed a stem-cell frequency of 1/21.7, whereas upon CHRDL1-depletion this is reduced 15-fold to

Preprints (www.preprints.org) | NOT PEER-REVIEWED | Posted: 20 October 2022 doi:10.20944/preprints202210.0308.v1

1/333.7. Since GS-5 GSCs grow considerably slower we further analyzed these cells after 1 week (Fig. 1C) for better comparison with NCH644 and to allow for sufficient sphere formation after an additional 2 weeks (Fig. 1D) of incubation. One week after seeding, GS-5 shCtrl revealed a calculated stem-cell-frequency of 1/404, whereas shCHRDL1 GS-5 had a 1.5 fold lower frequency of 1/600. This finding was further underscored after 2 weeks showing a stem-cell frequency of 1/75.5 of shCtrl GSCs, while shCHRDL1-GSCs had a 3.3-fold lower frequency of 1/248.7. Overall, we could show that CHRDL1-depletion reduces stemness.

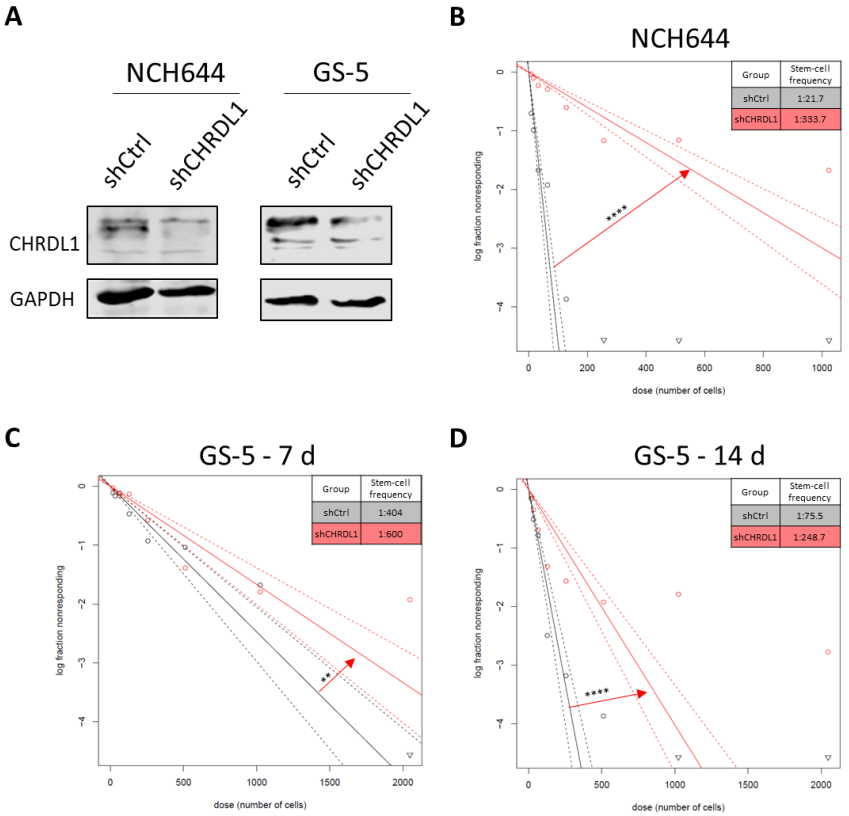

Figure 1. CHRDL1 depletion blocks stemness in GSCs. (A) Western Blot of NCH644 and GS-5 GSCs after stable transduction with a non-targeting shRNA (shCtrl) or specific shRNA targeting CHRDL1 (shCHRDL1). (B to D) Log-fraction plots of the limited dilution model of data from NCH644 shCtrl (black) and NCH644 shCHRDL1 (red) GSCs 7 days after seeding the cell in a dilution series from 1024 to 8 cells and analyzing the data using ELDA software [33]. (C and D) Data from GS-5 GSCs (C) 7 days and (D) 14 days after seeding of 2048 to 16 cells. **: $p<0.01$ ****: $p<0.0001$.

Based on these findings we next asked if this functional reduction of stemness is also associated with reduced expression of stemness-associated genes. For this purpose, we performed Taqman-based qRT-PCR in both NCH644 and GS-5. For NCH644 (Fig. 2) we could validate robust depletion of CHRDL1 mRNA expression upon shRNA-mediated CHRDL-KD (Fig. 2A). Similarly, we observed a prominent reduction of the stemness marker genes OLIG2 (Fig. 2B) and SOX2 (Fig. 2C), indicating reduced stemness. Curiously, SOX9 expression (Fig. 2D) shows a slight, but significant induction after CHRDL1-depletion. We further analyzed ZEB1 (Fig. 2E) and ZEB2 (Fig. 2F), which are associated with enhanced stemness, but also with an EMT-like phenotype and we observed a moderate, yet significant repression (ZEB1) and induction (ZEB2), respectively. The transmembrane protein CD44 (Fig. 2G) has also been associated with invasiveness of GBM cells and is considered a stemness marker and this gene was strongly reduced upon CHRDL1-KD, while intermediate filament NES (Nestin) is markedly strongly depleted (Fig. 2H). Finally, we analyzed a set of differentiation-associated genes. Upon CHRDL1-depletion the glial marker GFAP (Fig. 2I) as well as the neuronal marker NEFL (Neurofilament, Fig. 2J) are significantly upregulated, whereas MAP2 (Fig. 2K) only displays a tendency. Lastly,

Preprints (www.preprints.org) | NOT PEER-REVIEWED | Posted: 20 October 2022 doi:10.20944/preprints202210.0308.v1

RBFOXF3 (Fig. 2L), another neuronal marker is significantly increased. Collectively these data indicate that CHRDL1-depletion potently blocks several pathways associated with stemness and invasion, while inducing a more differentiated cellular state.

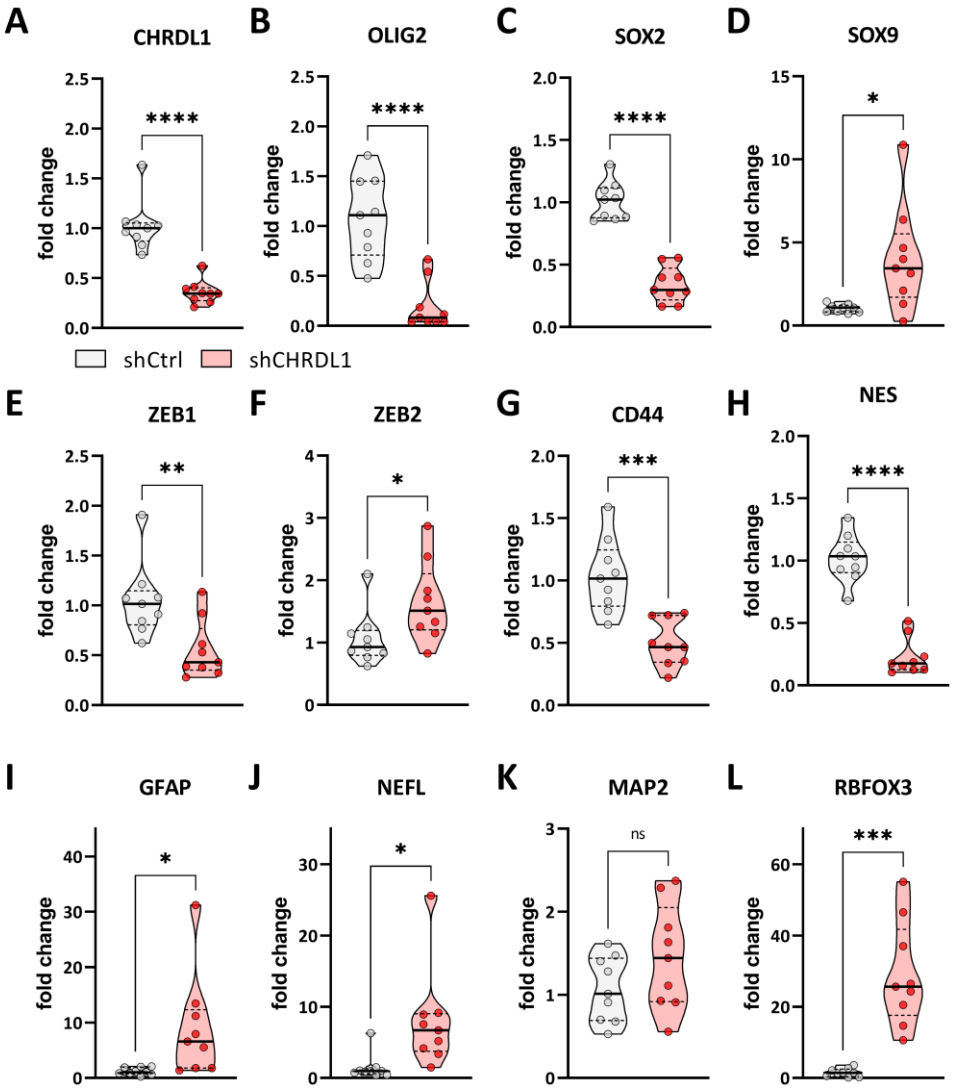

Figure 2. Point-plots of Taqman-based gene expression of NCH644 GSCs after stable transduction with a non-targeting shRNA (shCtrl) or specific shRNA targeting CHRDL1 (shCHRDL1) and measurement of (A) CHRDL1, (B) OLIG2, (C) SOX2, (D) SOX9, (E) ZEB1, (F) ZEB2, (G) CD44, (H) NES, (I) GFAP, (J) NEFL, (K) MAP2 and (L) RBFOX3 expression. The data are the summary of three experiments performed in triplicates. * $p < 0.05$; ** $p < 0.01$; *** $p < 0.001$; **** $p < 0.0001$; Unpaired t test with Welch's correction.

Like NCH644 we analyzed the same gene panel for GS-5 GSCs (Fig. 3) and firstly validated CHRDL1-depletion (Fig. 3A). Furthermore, we confirmed efficient depletion of the stemness-associated genes OLIG2 (Fig. 3B) and SOX2 (Fig. 3C), which is also accompanied by a significant reduction of SOX9 expression (Fig. 3D). The EMT-associated gene ZEB1 (Fig. 3E) is also significantly decreased, while ZEB2 (Fig. 3F) and CD44 (Fig. 3G) remain unchanged. The intermediate filament gene NES (Fig. 3H) only display a slight, but significant reduction after CHRDL1-depletion. Of the four differentiation markers GFAP (Fig. 3I), NEFL (Fig. 3J), MAP2 (Fig. 3K) and RBFOXF3 (Fig. 3L) neither shows a significant change, although GFAP and MAP2 show a slight tendency towards increased expression. In summary, we could validate our findings of grossly reduced stemness in a

Preprints (www.preprints.org) | NOT PEER-REVIEWED | Posted: 20 October 2022 doi:10.20944/preprints202210.0308.v1

second GSC line further underscoring that CHRDL1 could be a novel master regulator of GBM stemness.

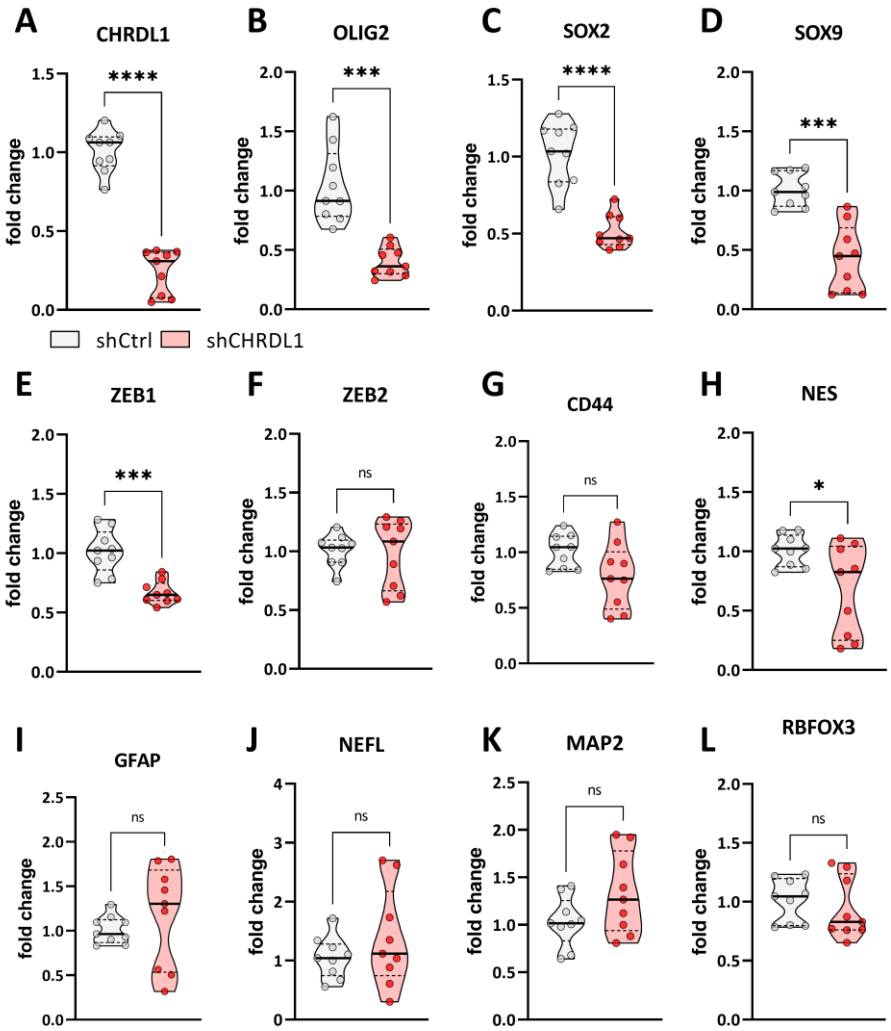

Figure 3. Point-plots of Taqman-based gene expression of GS-5 GSCs after stable transduction with a non-targeting shRNA (shCtrl) or specific shRNA targeting CHRDL1 (shCHRDL1) and measurement of (A) CHRDL1, (B) OLIG2, (C) SOX2, (D) SOX9, (E) ZEB1, (F) ZEB2, (G) CD44, (H) NES, (I) GFAP, (J) NEFL, (K) MAP2 and (L) RBFOX3 expression. The data are the summary of three experiments performed in triplicates.*** $p < 0.001$; **** $p < 0.0001$;ns: not significant unpaired t test with Welch's correction.

3.2. CHRDL1 depletion re-activates BMP4-signaling in GSCs

Based on the notion that a high CHRDL1-expression blocks BMP4 signaling and thereby enforces an enhanced stem-like state of GSCs, we first confirmed that NCH644 are proficient to relay BMP4-mediated signals by treating the cells with recombinant human BMP4 ligand (Fig. 4A). This showed us that upon BMP4-treatment pSMAD1/5 is highly increased, indicative of active BMP4-signaling. Similarly, CHRDL1-depleted NCH644 GSCs (Fig. 4B) also display increased pSMAD1/5 expression. Treatment of NCH644 and GS-5 GSCs with recombinant BMP4 (Fig. 4 C and D) resulted in reduced sphere forming potential in both GSCs, as did CHRDL1-depletion. The treatment of CHRDL1-depleted cells with rBMP4 led to no further enhancement in NCH644 compared to solvent-treated shCHRDL1 GSCs, whereas for GS-5 the combined approach further, potentially synergistically, reduced the sphere forming potential.

Preprints (www.preprints.org) | NOT PEER-REVIEWED | Posted: 20 October 2022 doi:10.20944/preprints202210.0308.v1

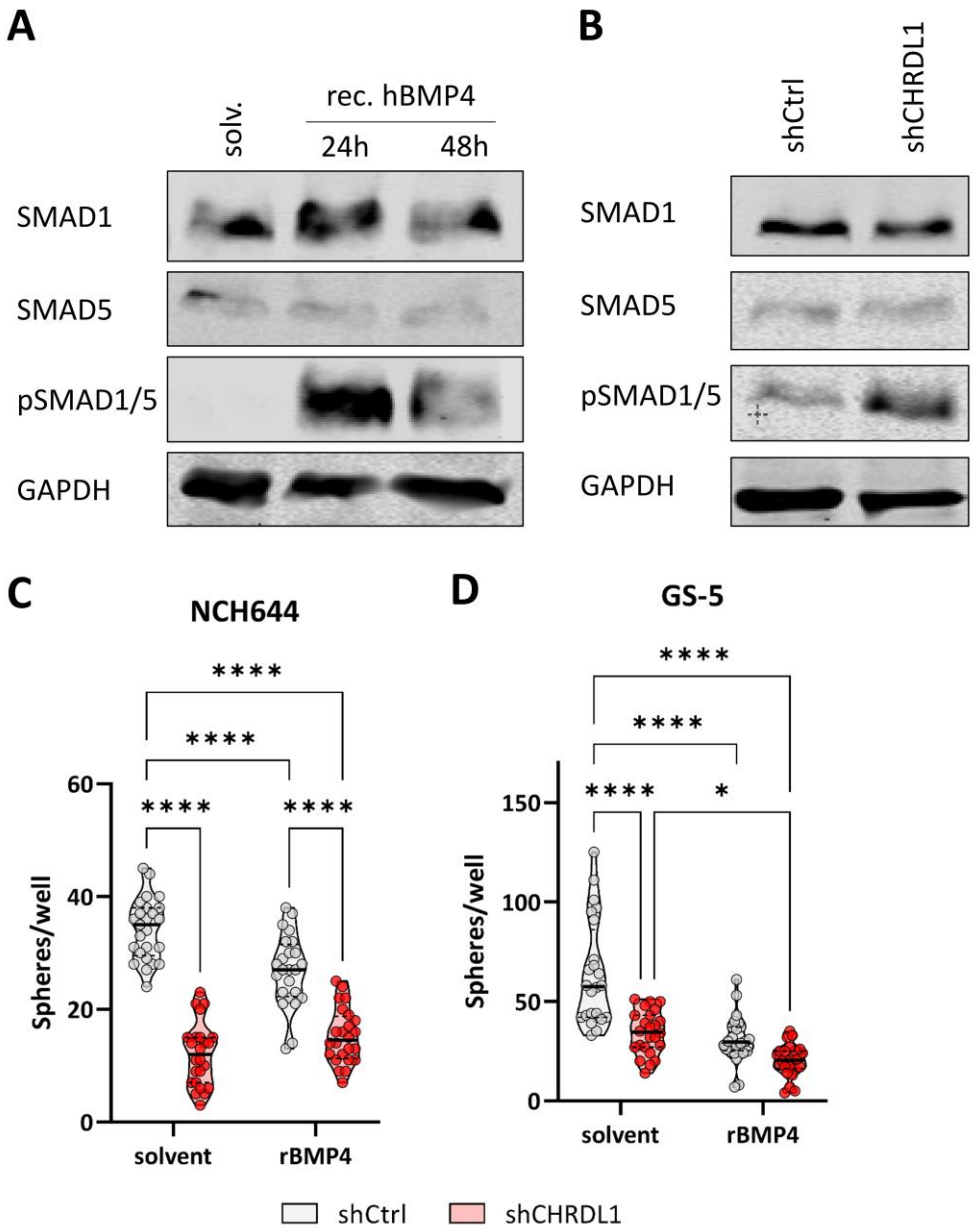

Figure 4. CHRDL1-depletion activates BMP4-signaling. (A and B) Western Blot of (A) NCH644 treated with 20 ng/ml recombinant human BMP4 for 24 or 48 h or (B) NCH644 shCtrl and shCHRDL1. (C and D) Sphere formation assay of (C) NCH644 and (D) GS-5 shCtrl or shCHRDL1 GSCs and treatment with 25 ng/ml recombinant BMP4 or solvent for 7 days after seeding of 500 and 1000cells per well. * $p < 0.05$; ** $p < 0.01$; *** $p < 0.001$; **** $p < 0.0001$; Two-Way-ANOVA with Sidak's multiple comparison tests.

3.3. CHRDL1 depletion sensitizes GSCs towards radiation treatment

Next, we reasoned that CHRDL1 depleted cells might be more vulnerable to conventional treatment, such as radiotherapy. For this purpose, we irradiated the cells with increased doses of X-ray (single-doses) and analyzed the amount of DNA double-strand breaks (DNA-DSB) using immunofluorescent staining against 53BP1 (Fig. 4A). We observed, significantly more 53BP1-positive foci, indicative of enhanced DNA damage, in CHRDL1-depleted cells mock irradiated and after irradiation with 2 Gy. After 4 Gy treatment no significant differences can be observed, whereas irradiation with 6 Gy significantly increases the amount of 53BP1 foci compared to non-irradiated GSCs. Hereafter, we reasoned that higher amounts of DNA-DSBs might lead to an enhanced growth inhibition and performed sphere formation assays of freshly dissociated GSCs seeded as single cells. This approach revealed that in CHRDL1-expressing NCH644 shCtrl cells every

Preprints (www.preprints.org) | NOT PEER-REVIEWED | Posted: 20 October 2022 doi:10.20944/preprints202210.0308.v1

IR dosage significantly impedes sphere formation. CHRDL1-depletion without irradiation (0 Gy) also significantly impedes sphere formation, basically confirming our results shown above. The combination of irradiation and CHRDL1 depletion can further block sphere formation after treatment with 6 Gy, thus reflecting the enhanced amount of DNA-DSBs.

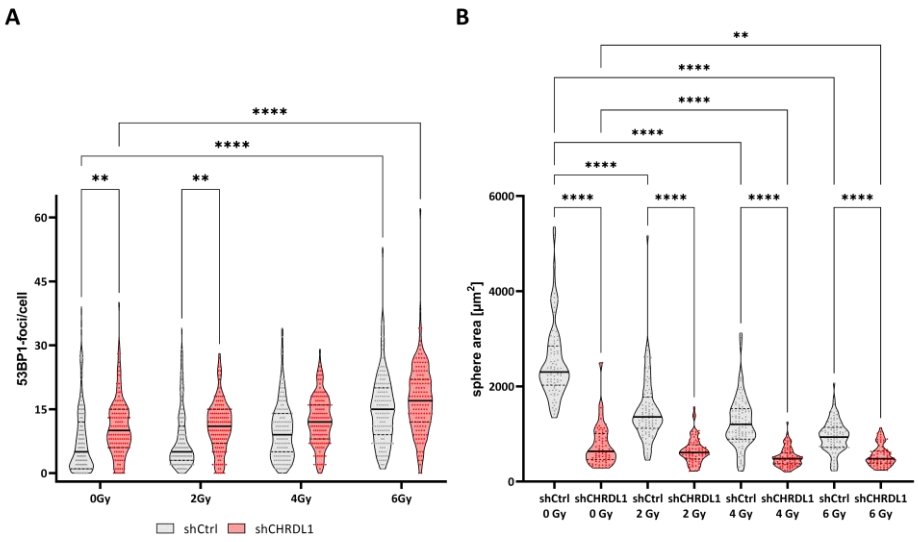

Figure 5. CHRDL1-depletion radiosensitizes GSCs. (A) 53BP1 foci assay 24h after irradiation of NCH644 shCtrl or NCH644 shCHRDL1 GSCs with the indicated doses. (B) Sphere formation of NCH644 shCtrl or shCHRDL1 cells 7 days after seeding of single cells and irradiation as indicated. * $p < 0.05$; ** $p < 0.01$; *** $p < 0.001$; **** $p < 0.0001$; Two-Way-ANOVA with Sidak's multiple comparison tests.

3.4. CHRDL1 is associated with poor prognosis in glioma and other cancers

Lastly, we interrogated the human protein atlas [37] in order to unravel the relevance of CHRDL1 for patient outcome and observed that high CHRDL1 expression is associated with worse clinical outcome in glioma (Fig. 5A), while it can also be considered unfavourable in urothelial (Fig. 5B) and renal cancer (Fig. 5C).

Preprints (www.preprints.org) | NOT PEER-REVIEWED | Posted: 20 October 2022 doi:10.20944/preprints202210.0308.v1

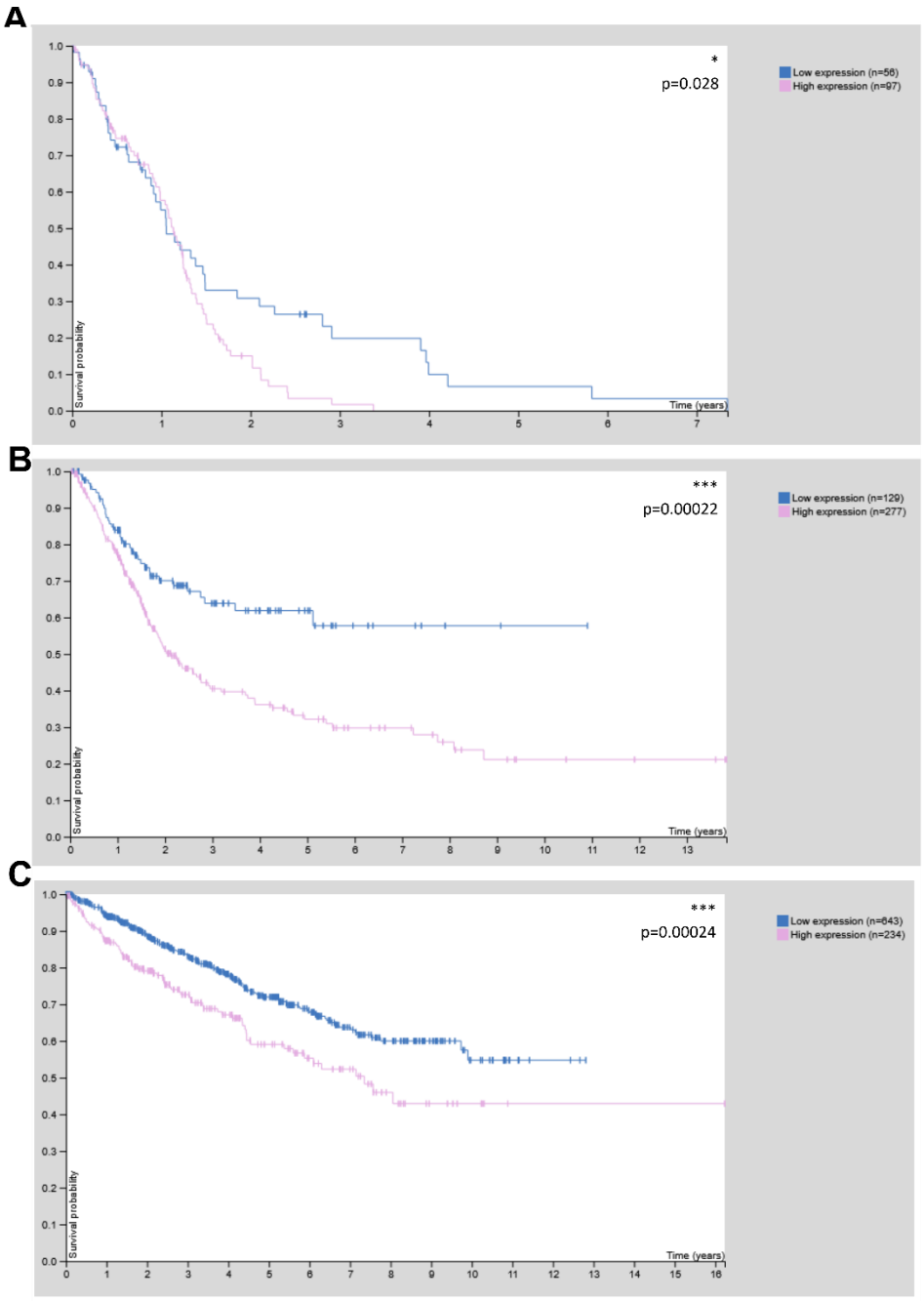

Figure 6. CHRDL1 is associated with worse survival in glioma (A) and an unfavourable prognosis in urothelial (B) and renal cancer (C) according to data from the human protein atlas [37]. * $p < 0.05$; ** $p < 0.01$; *** $p < 0.001$; **** $p < 0.0001$; log-rank p-value for Kaplan-Meier plot.

4. Discussion

Glioblastoma remains one of the most dismal cancer diagnosis of adults and current treatment strategies fail to cure the patients. It is hypothesized that this is largely due to stem-like states that can be obtained by some or all residual tumor cells that survive surgery and radiochemotherapy, resulting in more aggressive and ultimately lethal tumors. A better understanding of the underlying mechanisms is crucial to develop targeted and patient-centered approaches that can be based on the molecular knowledge of different tumor types.

BMP4 has been shown to enforce differentiation of GSCs almost 2 decades ago and has been tested as "differentiation therapy" [21]. Although this notion has not been fulfilled and the entire concept of stable differentiation has been challenged, particularly due to the presence of different, highly plastic cell states that might be driven by different

molecular alterations [8-10], the question remains as to how tumor cells evade these stemness-blocking cues. One factor that has been shown recently to be overexpressed in cancers, including GBM is the secreted BMP4 antagonist CHRDL1 [24,25]. Accordingly, our working hypothesis was that CHRDL1 acts as an enforcer of stemness in GSCs. Within this report we employed two previously described GSCs spheroid cultures [27,28] and depleted them of CHRDL1 using stable transduction of a CHRDL1-targeting shRNA. This CHRDL1-depletion was accompanied by functional, as well as molecular changes that conclusively can be interpreted as stemness blockade. Further considering that GSCs are known to be more resistant towards conventional therapy such as radiotherapy, we could further confirm that CHRDL1-depleted cells are indeed sensitized for IR treatment.

Very recently, it was shown in diffuse intrinsic pontine glioma, a very aggressive juvenile glioma type, that activation of BMP signalling enforces cellular differentiation similar to our findings presented in the current study. Mechanistically it was shown that upregulation of CHRDL1 expression results in counteraction of the tumor-suppressive effects of BMP4 and that depletion of CHRDL1 significantly reduced cell proliferation and sphere formation as well as tumor growth in a xenograft model[38]. The authors showed also, that BMP4 treatment of diffuse intrinsic pontine glioma (DIPG) cells induced a stemness-blockade accompanied by decreased SOX2 and OLIG2 expression further validating our findings. Mechanistically the authors proposed that by epigenetic upregulation of the tumor suppressor CXXC5 the BMP4-response is mediated [38]. Taken into account these studies, one may propose that (re-) activation of BMP4 signalling might be a suitable strategy to block the stem-like phenotype of adult and juvenile gliomas and thereby sensitizing them towards conventional therapy regimes. In our study, we found additional evidence that high CHRDL1-expression might serve as a marker protein to determine BMP4-susceptibility. Whether this mechanism might also be expanded to other tumor entities should also be investigated in future studies. For example is it know that BMP4 can exert pro-tumorigenic functions in breast cancer, where it mediates migration and invasion, which can be blocked via CHRDL1 [25], whereas CHRDL1 induces neuronal differentiation of neural stem cells [26]. Accordingly, the origin and/or location of the tumor likely dictates how external cues are perceived.

Clinically it is interesting to note that CHRDL1 is, according to data from the human protein atlas, associated with worse survival in glioma, as well as in urothelial and renal cancer. One could therefore hypothesize that CHRDL1 has potential as a prognostic factor that could be considered in routine diagnostics. According to the literature is CHRDL1 associated with worse prognosis in oral squamous cell carcinoma [39], where it also regulates metastasis and EMT [40].

Interestingly, astrocytes are also able to secrete CHRDL1 during the physiological process of wound healing after ischemic injury to facilitate the healing process [41]. This leaves the open questions on where CHRDL1 originates in a multicellular tumor and how it affects non-tumor cells. Using more complex model system, such as organotypic brain slice culture or even in vivo approaches these questions should be addressed in future studies and ways to target CHRDL1 in a cell-autonomous way, e.g., via targeting antibodies, should be explored.

Funding: This study is supported by a grant from the Deutsche Forschungsgemeinschaft (German Research Foundation, DFG) to Benedikt Linder (Grant: LI 3687/2-1).

Institutional Review Board Statement: Not applicable

Informed Consent Statement: Not applicable

Data Availability Statement: No large-scale datasets have been generated. Raw data of the experiments and/or materials can be provided upon reasonable request.

Acknowledgments: We would like to thank Hildegard König for her ongoing excellent technical assistance. Furthermore, we thank Andrej Wehle who helped establish the viral transduction procedure.

Conflicts of Interest: The authors declare no conflict of interest

References

1. Louis, D.N.; Perry, A.; Reifenberger, G.; von Deimling, A.; Figarella-Branger, D.; Cavenee, W.K.; Ohgaki, H.; Wiestler, O.D.; Kleihues, P.; Ellison, D.W. The 2016 World Health Organization Classification of Tumors of the Central Nervous System: a summary. Acta Neuropathol 2016, 131, 803-820, doi:10.1007/s00401-016-1545-1.
2. Louis, D.N.; Perry, A.; Wesseling, P.; Brat, D.J.; Cree, I.A.; Figarella-Branger, D.; Hawkins, C.; Ng, H.K.; Pfister, S.M.; Reifenberger, G., et al. The 2021 WHO Classification of Tumors of the Central Nervous System: a summary. Neuro Oncol 2021, 23, 1231-1251, doi:10.1093/neuonc/noab106.
3. Stupp, R.; Hegi, M.E.; Gilbert, M.R.; Chakravarti, A. Chemoradiotherapy in malignant glioma: standard of care and future directions. J Clin Oncol 2007, 25, 4127-4136, doi:10.1200/JCO.2007.11.8554.
4. Stupp, R.; Mason, W.P.; van den Bent, M.J.; Weller, M.; Fisher, B.; Taphoorn, M.J.; Belanger, K.; Brandes, A.A.; Marosi, C.; Bogdahn, U., et al. Radiotherapy plus concomitant and adjuvant temozolomide for glioblastoma. N Engl J Med 2005, 352, 987-996, doi:10.1056/NEJMoa043330.
5. Stupp, R.; Hegi, M.E.; Mason, W.P.; van den Bent, M.J.; Taphoorn, M.J.; Janzer, R.C.; Ludwin, S.K.; Allgeier, A.; Fisher, B.; Belanger, K., et al. Effects of radiotherapy with concomitant and adjuvant temozolomide versus radiotherapy alone on survival in glioblastoma in a randomised phase III study: 5-year analysis of the EORTC-NCIC trial. Lancet Oncol 2009, 10, 459-466, doi:10.1016/S1470-2045(09)70025-7.
6. Luwor, R.B.; Baradaran, B.; Taylor, L.E.; Iaria, J.; Nheu, T.V.; Amiry, N.; Hovens, C.M.; Wang, B.; Kaye, A.H.; Zhu, H.J. Targeting Stat3 and Smad7 to restore TGF-beta cytostatic regulation of tumor cells in vitro and in vivo. Oncogene 2013, 32, 2433-2441, doi:10.1038/onc.2012.260.
7. Butler, M.; Pongor, L.; Su, Y.T.; Xi, L.; Raffeld, M.; Quezado, M.; Trepel, J.; Aldape, K.; Pommier, Y.; Wu, J. MGMT Status as a Clinical Biomarker in Glioblastoma. Trends Cancer 2020, 6, 380-391, doi:10.1016/j.trecan.2020.02.010.
8. Tirosh, I.; Venteicher, A.S.; Hebert, C.; Escalante, L.E.; Patel, A.P.; Yizhak, K.; Fisher, J.M.; Rodman, C.; Mount, C.; Filbin, M.G., et al. Single-cell RNA-seq supports a developmental hierarchy in human oligodendroglioma. Nature 2016, 539, 309-313, doi:10.1038/nature20123.
9. Neftel, C.; Laffy, J.; Filbin, M.G.; Hara, T.; Shore, M.E.; Rahme, G.J.; Richman, A.R.; Silverbush, D.; Shaw, M.L.; Hebert, C.M., et al. An Integrative Model of Cellular States, Plasticity, and Genetics for Glioblastoma. Cell 2019, 178, 835-849 e821, doi:10.1016/j.cell.2019.06.024.
10. Dirkse, A.; Golebiewska, A.; Buder, T.; Nazarov, P.V.; Muller, A.; Poovathingal, S.; Brons, N.H.C.; Leite, S.; Sauvageot, N.; Sarkisjan, D., et al. Stem cell-associated heterogeneity in Glioblastoma results from intrinsic tumor plasticity shaped by the microenvironment. Nat Commun 2019, 10, 1787, doi:10.1038/s41467-019-09853-z.
11. Krakstad, C.; Chekenya, M. Survival signalling and apoptosis resistance in glioblastomas: opportunities for targeted therapeutics. Mol Cancer 2010, 9, 135, doi:10.1186/1476-4598-9-135.
12. Bradshaw, A.; Wickremsekera, A.; Tan, S.T.; Peng, L.; Davis, P.F.; Itinteang, T. Cancer Stem Cell Hierarchy in Glioblastoma Multiforme. Front Surg 2016, 3, 21, doi:10.3389/fsurg.2016.00021.
13. Bao, S.; Wu, Q.; McLendon, R.E.; Hao, Y.; Shi, Q.; Hjelmeland, A.B.; Dewhirst, M.W.; Bigner, D.D.; Rich, J.N. Glioma stem cells promote radioresistance by preferential activation of the DNA damage response. Nature 2006, 444, 756-760, doi:10.1038/nature05236.
14. Schiffer, D.; Mellai, M.; Annovazzi, L.; Caldera, V.; Piazzi, A.; Denysenko, T.; Melcarne, A. Stem cell niches in glioblastoma: a neuropathological view. Biomed Res Int 2014, 2014, 725921, doi:10.1155/2014/725921.
15. Signore, M.; Ricci-Vitiani, L.; De Maria, R. Targeting apoptosis pathways in cancer stem cells. Cancer Lett 2013, 332, 374-382, doi:10.1016/j.canlet.2011.01.013.
16. Pollard, S.M.; Yoshikawa, K.; Clarke, I.D.; Danovi, D.; Stricker, S.; Russell, R.; Bayani, J.; Head, R.; Lee, M.; Bernstein, M., et al. Glioma stem cell lines expanded in adherent culture have tumor-specific phenotypes and are suitable for chemical and genetic screens. Cell Stem Cell 2009, 4, 568-580, doi:10.1016/j.stem.2009.03.014.
17. Liu, Y.; Liu, X.; Chen, L.-C.; Du, W.-Z.; Cui, Y.-Q.; Piao, X.-Y.; Li, Y.-L.; Jiang, C.-L. Targeting glioma stem cells via the Hedgehog signaling pathway. Neuroimmunology and Neuroinflammation 2014, 10.4103/2347-8659.139715, 51, doi:10.4103/2347-8659.139715.
18. Gilbert, C.A.; Ross, A.H. Cancer stem cells: cell culture, markers, and targets for new therapies. J Cell Biochem 2009, 108, 1031-1038, doi:10.1002/jcb.22350.
19. Linder, B.; Wehle, A.; Hehlgans, S.; Bonn, F.; Dikic, I.; Rodel, F.; Seifert, V.; Kogel, D. Arsenic Trioxide and (-)-Gossypol Synergistically Target Glioma Stem-Like Cells via Inhibition of Hedgehog and Notch Signaling. Cancers (Basel) 2019, 11, doi:10.3390/cancers11030350.
20. Kane, R.; Godson, C.; O'Brien, C. Chordin-like 1, a bone morphogenetic protein-4 antagonist, is upregulated by hypoxia in human retinal pericytes and plays a role in regulating angiogenesis. Mol Vis 2008, 14, 1138-1148.
21. Piccirillo, S.G.; Reynolds, B.A.; Zanetti, N.; Lamorte, G.; Binda, E.; Broggi, G.; Brem, H.; Olivi, A.; Dimeco, F.; Vescovi, A.L. Bone morphogenetic proteins inhibit the tumorigenic potential of human brain tumour-initiating cells. Nature 2006, 444, 761-765, doi:10.1038/nature05349.
22. Koguchi, M.; Nakahara, Y.; Ito, H.; Wakamiya, T.; Yoshioka, F.; Ogata, A.; Inoue, K.; Masuoka, J.; Izumi, H.; Abe, T. BMP4 induces asymmetric cell division in human glioma stem-like cells. Oncol Lett 2020, 19, 1247-1254, doi:10.3892/ol.2019.11231.

23. Sachdeva, R.; Wu, M.; Johnson, K.; Kim, H.; Celebre, A.; Shahzad, U.; Graham, M.S.; Kessler, J.A.; Chuang, J.H.; Karamchandani, J., et al. BMP signaling mediates glioma stem cell quiescence and confers treatment resistance in glioblastoma. Sci Rep 2019, 9, 14569, doi:10.1038/s41598-019-51270-1.
24. Itoh, N.; Ohta, H. Secreted bone morphogenetic protein antagonists of the Chordin family. Biomol Concepts 2010, 1, 297-304, doi:10.1515/bmc.2010.026.
25. Cyr-Depauw, C.; Northey, J.J.; Tabaries, S.; Annis, M.G.; Dong, Z.; Cory, S.; Hallett, M.; Rennhack, J.P.; Andrechek, E.R.; Siegel, P.M. Chordin-Like 1 Suppresses Bone Morphogenetic Protein 4-Induced Breast Cancer Cell Migration and Invasion. Mol Cell Biol 2016, 36, 1509-1525, doi:10.1128/MCB.00600-15.
26. Gao, W.L.; Zhang, S.Q.; Zhang, H.; Wan, B.; Yin, Z.S. Chordin-like protein 1 promotes neuronal differentiation by inhibiting bone morphogenetic protein-4 in neural stem cells. Mol Med Rep 2013, 7, 1143-1148, doi:10.3892/mmr.2013.1310.
27. Campos, B.; Wan, F.; Farhadi, M.; Ernst, A.; Zeppernick, F.; Tagscherer, K.E.; Ahmadi, R.; Lohr, J.; Dictus, C.; Gdynia, G., et al. Differentiation therapy exerts antitumor effects on stem-like glioma cells. Clin Cancer Res 2010, 16, 2715-2728, doi:10.1158/1078-0432.CCR-09-1800.
28. Gunther, H.S.; Schmidt, N.O.; Phillips, H.S.; Kemming, D.; Kharbanda, S.; Soriano, R.; Modrusan, Z.; Meissner, H.; Westphal, M.; Lamszus, K. Glioblastoma-derived stem cell-enriched cultures form distinct subgroups according to molecular and phenotypic criteria. Oncogene 2008, 27, 2897-2909, doi:10.1038/sj.onc.1210949.
29. Gerstmeier, J.; Possmayer, A.L.; Bozkurt, S.; Hoffmann, M.E.; Dikic, I.; Herold-Mende, C.; Burger, M.C.; Munch, C.; Kogel, D.; Linder, B. Calcitriol Promotes Differentiation of Glioma Stem-Like Cells and Increases Their Susceptibility to Temozolomide. Cancers (Basel) 2021, 13, doi:10.3390/cancers13143577.
30. Remy, J.; Linder, B.; Weirauch, U.; Day, B.W.; Stringer, B.W.; Herold-Mende, C.; Aigner, A.; Krohn, K.; Kogel, D. STAT3 Enhances Sensitivity of Glioblastoma to Drug-Induced Autophagy-Dependent Cell Death. Cancers (Basel) 2022, 14, doi:10.3390/cancers14020339.
31. Linder, B.; Kohler, L.H.F.; Reisbeck, L.; Menger, D.; Subramaniam, D.; Herold-Mende, C.; Anant, S.; Schobert, R.; Biersack, B.; Kogel, D. A New Pentafluorothio-Substituted Curcuminoid with Superior Antitumor Activity. Biomolecules 2021, 11, doi:10.3390/biom11070947.
32. Rahman, M.; Reyner, K.; Deleyrolle, L.; Millette, S.; Azari, H.; Day, B.W.; Stringer, B.W.; Boyd, A.W.; Johns, T.G.; Blot, V., et al. Neurosphere and adherent culture conditions are equivalent for malignant glioma stem cell lines. Anat Cell Biol 2015, 48, 25-35, doi:10.5115/acb.2015.48.1.25.
33. Hu, Y.; Smyth, G.K. ELDA: extreme limiting dilution analysis for comparing depleted and enriched populations in stem cell and other assays. J Immunol Methods 2009, 347, 70-78, doi:10.1016/j.jim.2009.06.008.
34. Gilbert, C.A.; Daou, M.C.; Moser, R.P.; Ross, A.H. Gamma-secretase inhibitors enhance temozolomide treatment of human gliomas by inhibiting neurosphere repopulation and xenograft recurrence. Cancer Res 2010, 70, 6870-6879, doi:10.1158/0008-5472.CAN-10-1378.
35. Schindelin, J.; Arganda-Carreras, I.; Frise, E.; Kaynig, V.; Longair, M.; Pietzsch, T.; Preibisch, S.; Rueden, C.; Saalfeld, S.; Schmid, B., et al. Fiji: an open-source platform for biological-image analysis. Nat Methods 2012, 9, 676-682, doi:10.1038/nmeth.2019.
36. Antonietti, P.; Linder, B.; Hehlgans, S.; Mildenberger, I.C.; Burger, M.C.; Fulda, S.; Steinbach, J.P.; Gessler, F.; Rodel, F.; Mittelbronn, M., et al. Interference with the HSF1/HSP70/BAG3 Pathway Primes Glioma Cells to Matrix Detachment and BH3 Mimetic-Induced Apoptosis. Mol Cancer Ther 2017, 16, 156-168, doi:10.1158/1535-7163.MCT-16-0262.
37. Uhlen, M.; Zhang, C.; Lee, S.; Sjostedt, E.; Fagerberg, L.; Bidkhori, G.; Benfeitas, R.; Arif, M.; Liu, Z.; Edfors, F., et al. A pathology atlas of the human cancer transcriptome. Science 2017, 357, doi:10.1126/science.aan2507.
38. Sun, Y.; Yan, K.; Wang, Y.; Xu, C.; Wang, D.; Zhou, W.; Guo, S.; Han, Y.; Tang, L.; Shao, Y., et al. Context-dependent tumor-suppressive BMP signaling in diffuse intrinsic pontine glioma regulates stemness through epigenetic regulation of CXXC5. Nat Cancer 2022, 3, 1105-1122, doi:10.1038/s43018-022-00408-8.
39. Han, Y.; Xia, L.; Wang, X.; Xiong, H.; Zeng, L.; Wang, Z.; Zhang, T.; Xia, K.; Hu, X.; Su, T. Study on the expression and function of chordin-like 1 in oral squamous cell carcinoma. Oral Dis 2022, 10.1111/odi.14240, doi:10.1111/odi.14240.
40. Wu, Q.; Zheng, Z.; Zhang, J.; Piao, Z.; Xin, M.; Xiang, X.; Wu, A.; Zhao, T.; Huang, S.; Qiao, Y., et al. Chordin-Like 1 Regulates Epithelial-to-Mesenchymal Transition and Metastasis via the MAPK Signaling Pathway in Oral Squamous Cell Carcinoma. Front Oncol 2022, 12, 862751, doi:10.3389/fonc.2022.862751.
41. Blanco-Suarez, E.; Allen, N.J. Astrocyte-secreted chordin-like 1 regulates spine density after ischemic injury. Sci Rep 2022, 12, 4176, doi:10.1038/s41598-022-08031-4.